Volume 9, Issue 2, 2020, 1022 - 1028 ISSN 2284-6808

Letters in Applied NanoBioScience

https://nanobioletters.com/

https://doi.org/10.33263/LIANBS92.10221028

Original Research Article Open Access Journal

Received: 17.04.2020 / Revised: 07.05.2020 / Accepted: 07.05.2020 / Published on-line: 10.05.2020

Comparative study on antimicrobial activities of green synthesized TiO_2 nanoparticles of *Tephrosia purpurea* leaves with its crude extracts

Neelesh Babu [1, *], Navneet Kumar [1]

[1] Department of Botany and Microbiology, Gurukula Kangri Vishwavidyalaya Haridwar, India

*corresponding author e-mail address: ***sonkarneil@gmail.com***

ABSTRACT

The present study deals with the enhancement of antimicrobial potential of *Tephrosia purpurea* crude extracts by making their composite with TiO_2 nanoparticles against ubiquitous pathogens which may cause skin and wound infections. The synthesis was accomplished by the sol-gel method using precursor Titanium isopropoxide. The nanoparticles characterized by XRD, FESEM and FTIR techniques. XRD results showed that particles were in anatase phase with average crystallite size 12- 24 nm. FESEM reveals the spherical surface morphology of the nanoparticles. FTIR spectra gave the idea about associated functional groups with the synthesized particles. The antimicrobial potential of chemically synthesized TiO_2 nanoparticles, green synthesized TiO_2 nanoparticles and the crude extracts tested against *Escherichia coli* MTCC 40, *Pseudomonas aeruginosa* MTCC 2474 and *Streptococcus pyogenes* MTCC 442 which are actively involved in skin and wound infections. Results showed that green synthesized TiO2 nanoparticles gave better results in comparison with chemically synthesized TiO_2 nanoparticles and crude extracts.

Keywords: *Titanium dioxide; Green synthesis; Sol-gel; Nanoparticles; Wound infection; Antimicrobial activity; Plant extracts; Tephrosiapurpurea.*

Abbreviations

TiO_2/PE - Green synthesized nanoparticles by petroleum ether extract
TiO_2/BZ - Green synthesized nanoparticles by benzene extract
TiO_2/MeOH - Green synthesized nanoparticles by methanol extract
TiO_2/W - Green synthesized nanoparticles by water extract

1. INTRODUCTION

The nanoparticles-based drug delivery systems have been developed by the great efforts which employ nanostructured materials made by the combination of bioactive compounds and inorganic nanostructured matrix. Metal nanoparticles are enormously used because of their unique physical and chemical properties and widely used in various areas such as antibacterial, antiviral, diagnostics, anticancer and targeted drug delivery [1]. They may combine biopolymers that mimic the organic components of the extracellular matrix of bone and bioactive nanoceramics to induce biomineralization [2]. The antimicrobial activity of nanoparticles either directly interact with the microbial cells (interrupting transmembrane electron transfer, disrupting/penetrating the cell envelope, or oxidizing cell components) or produce secondary products [3]. Titanium dioxide is one of the most studied semiconductors for photo-catalytic reactions due to its low cost, ease of handling and high resistance to photo-induced decomposition [4]. These metal nanoparticles have the advantages of both cheapness and non-toxicity, in addition to its excellent functionality and long-term stability. Because of these properties, it has been approved by the American Food and Drug Administration (FDA) for use in human food, drugs, cosmetics and food contact materials [5]. TiO_2 also exhibits bactericidal activity when it irradiated with near-UV light [6]. The present study deals with the green synthesis of TiO_2 nanoparticles using the different extracts of *Tephrosia purpurea* herb. We aimed at using *Tephrosia purpurea* for the first time and standardizing the TiO_2 synthesis protocol using its leaves extracts and titanium isopropoxide.

Tephrosia purpurea belongs to family Fabaceae and used traditionally as a folk medicine because of its several properties such as anticancer, antipyretic, antidiabetic, antiviral, antimicrobial, anti-inflammatory etc. This herb is effectively utilized as folkloric medicine for the treatment of inflammation as well as enlargement of liver and spleen. It also has the potential of pro-healing and able to improve collagen maturation by cross-linking. Its antioxidants help to prevent the damage caused by free radicals by quenching superoxide radicals [7]. Several studies showed that this plant works as a potent antimicrobial agent against several pathogens associated with wound and other infections [8].

2. MATERIALS AND METHODS

2.1. Materials.

The herb *Tephrosia purpurea* collected from bare land beside Gurukula Kangri University, Haridwar, Uttarakhand and further authenticated from Botanical Survey of India, Dehradun, Uttarakhand is having accession number 116607. Titanium precursor (Titanium isopropoxide) and ethanol purchased from Sigma Aldrich and Merk. Different solvents (petroleum ether, benzene and methanol) and culture media (Muller Hilton agar and Nutrient broth) were bought from CDH (Central Drug House) New Delhi. Three different bacterial strains *Escherichia coli* MTCC 40,

Pseudomonas aeruginosa MTCC 2474 and *Streptococcus pyogenes* MTCC 442 associated with wound infections used. Powdered XRD, FTIR and FE-SEM analyzed all the composites and chemically synthesized TiO2. X-ray diffraction patterns were recorded by Bruker AXS D8- Advanced diffractometer with Cu-Kα radiation (λ= 1.5406 Å) in the 2Θ range 20˚- 80˚. For the FTIR analysis, Perkin Elmer spectrum two spectrometer was used in particle range 400 – 4000 cm-1. Surface morphology of the samples was recorded by Carl Zeiss Ultra plus Field-Emission Scanning Electron Microscope with an accelerated voltage of 15.00 Kv in high vacuum mode to achieve maximum magnification between 100X- 100,000X. UV - Visible spectra analyzed by Systronics UV - Visible spectrometer in the range 200-800 nm.

2.2. Extraction.

The leaves of the plant were shade dried at room temperature for 15 days. Dried leaves were coarsely powdered, and the quantity of 200 g filled in Soxhlet apparatus. The extractions were carried out by four different solvents (350 ml each), i.e. petroleum ether, benzene, methanol and water [9].

2.3. Chemical synthesis of TiO_2

Titania nanoparticles prepared by the sol-gel method where Titanium isopropoxide (Sigma Aldrich >97%) used as titanium precursor. The synthesis carried out as the method descibed by Liu et al., (2003) with few modifications [10]. Titanium precursor dissolved in ethanol (Merck) in the ratio 1:2 then the suspension was added drop wise to the mixture containing alcohol, hydrochloric acid and deionised water under vigorous stirring at room temperature. After 2 hours, the solution gradually turned into a yellowish gel which further precipitated. The resulting precipitate was recovered by centrifugation with repeated washings by ethanol and dried at 70˚C followed by crushing with mortar and pestle. The dried powder calcinated in the muffle furnace at 500˚C. Figure (1).

2.4. Green synthesis of TiO_2

For the green synthesis, 500 mg of plant extract suspended in 10 ml of ethanol and the suspension further mixed with 5 ml of titanium isopropoxide. The mixture added dropwise to the solution containing ethanol, HCl and deionised water (30:1.66:1) under vigorous stirring at room temperature for two hours. Similar to the chemical synthesis resulting precipitate was further recovered and calcinated.

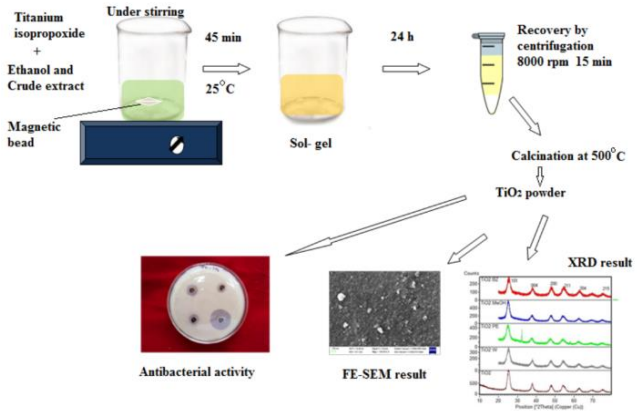

Figure 1. Graphical abstract of the synthesis of titanium dioxide nanoparticles via sol-gel method.

2.5. Antibacterial activity.

Lyophilized bacterial cultures purchased from MTCC were suspended into the nutrient broth with 0.5% NaCl at 37˚C for 24 h. The bacterial inoculums for the antibacterial activity prepared by adjusting turbidity according to McFarland standards 0.5 in nutrient broth. Antibacterial activities of the samples measured by the well diffusion method. Four wells having the diameter 6 mm were punched by sterile cork borer on Muller Hilton agar plates and further seeded with stock bacterial cultures [11]. The powdered nanoparticles composites suspended in distilled water in the concentration 50 µg/ml, which kept under UV light for 1 hour and 45 µl of each sample poured into the wells. Similarly, four different extracts were suspended in DMSO in the concentration of 50µg/ml each and tested against given test organisms. Antibiotic disks of cefazolin (30mcg), streptomycin (10 mcg) and ampicillin (10 mcg) were used as a positive control, whereas distilled water and DMSO considered as the negative controls. All the plates were tested in triplicates and subjected for the incubation at 37˚C for 24 hours. The results recorded through the zone of inhibition in mm.

3. RESULTS

3.1. Characterization.

The structure and crystallinity of chemically synthesized TiO_2 and TiO_2/plants extract composites analyzed by X-ray diffraction. Figure (2) shows resultant peaks which confirm the presence of TiO_2 in the samples. The peaks were in good agreement and matched with the standard results of anatase phase (JCPDS card no. 21- 1272). An increase in the width of peak results in a decrease in the size of particles. The average crystallite size of the particles in nm calculated by using the Scherer formula.

$$d = \frac{0.9\lambda}{\beta cos\theta}$$

Where, d= Mean diameter of the particles
λ = Wavelength of the radiation.
β =Angular FWHM of peak
Θ = Diffraction angle.

The XRD pattern of chemically synthesized TiO_2 and TiO_2/plant extracts composites shows peaks of anatase phase with a reflection on 101, 004, 200, 211, 204 and 215. The average crystallite size of chemically synthesized TiO_2 nanoparticles ranges between 12- 22 nm while TiO_2/petroleum ether extract, TiO2/benzene extract, TiO_2/methanol extract and TiO_2/water extract were 15- 25 nm, 12- 24 nm, 12-15 nm and 14- 24 nm respectively. Similar results obtained in previous studies. Maurya et al., (2012) calculated the 6- 20 nm size of green synthesized TiO_2 by Bauhinia variegate using Scherer formula [12]. In another study, Amanulla and Sundaram (2019) obtained 17-21 nm-sized TiO_2 nanoparticles synthesized using orange peel extract [13].

Surface morphology of the samples obtained by FESEM shown in figure 3(a), 3(b), 3(c), 3(d) and 3(e). FESEM images on the resolution of 100 nm revealed the formation of spherical shaped particles in agglomerated form. Basically agglomeration of the particles is due to their high surface energy and van der Waals attraction of forces between them. To reduce their high surface energy, they tend to agglomerate [14]. The average grain size of the particles was 12-24 nm measured by Image J software which favours the results obtained by XRD and revealed that particles were in the nano range. Bottom-up approaches employed for the morphology and size-controlled nanoparticles synthesis as it builds

up from the atom by atom. Primarily these processes produce spherical to near-spherical shaped nanoparticles. Sol-gel is one of these processes which are widely employed. It generally utilizes sol or colloidal suspension formed from the hydrolysis and polymerization of the inorganic metal salt. Homogenous nucleation during the synthesis causes spherical shaped particles [15, 16].

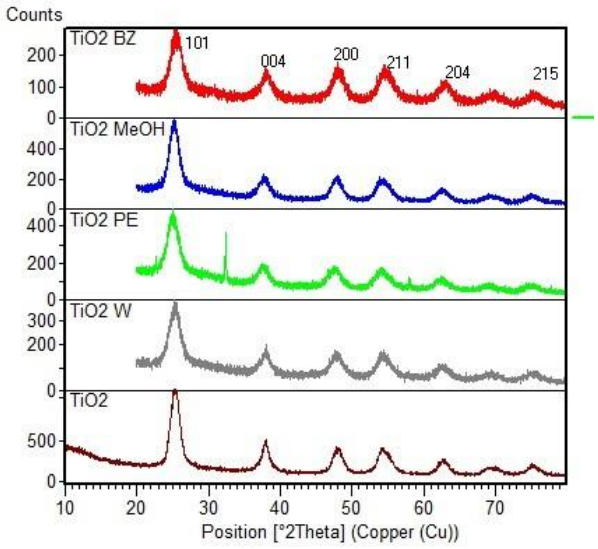

Figure 2. XRD patterns of Titanium dioxide nanoparticles TiO_2/BZ, TiO_2/MeOH, TiO_2/PE, TiO_2/W and TiO_2 (Green synthesized by benzene, methanol, petroleum ether and water extracts of Tephrosia purpura leaves and chemically synthesized).

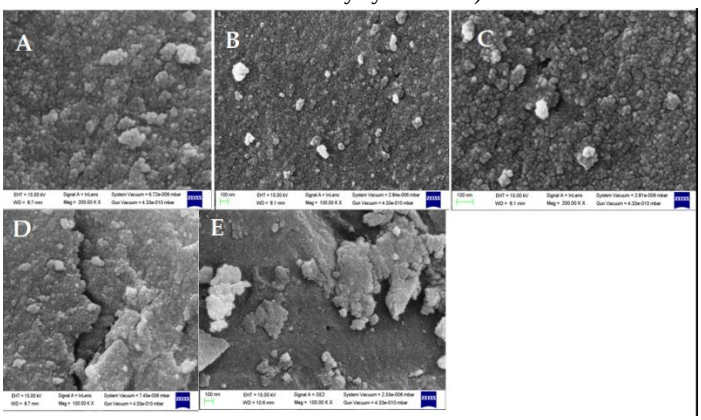

Figure 3. FESEM images of (a) chemically synthesized TiO_2, (b) green synthesized TiO_2 /P.E, (c) green synthesized TiO_2 /BZ,(d) green synthesized TiO_2 /MeOH and (e) green synthesized TiO_2 /W.

In figure 4 five spectrums (TiO_2, TiO_2 /PE, TiO_2 /BZ, TiO_2 /MeOH and TiO_2 /W) showed FTIR peaks. The technique used to determine the associated functional groups worked as a capping agent during the green synthesis of TiO_2. The origin of vibrational bands are as follows: bands observed at 3524 cm^{-1}, 3500 cm^{-1}, 3413 cm^{-1}, 3400 cm^{-1} shows OH stretching vibrations of TiO_2 nanoparticles [17, 18]. At 3195cm^{-1} symmetrical stretching of N-H, 1701cm^{-1}, 1709 $cm^{-1}$and 1713 cm^{-1} shows stretching C=O vibrations which are H-bonded. Changes in C=O vibrations could be connected with the destruction of old OH bonds and the creation of new ones [17]. 1636 cm^{-1}, 1625 cm^{-1} corresponds to bending modes of Ti-OH [18]. 1400 cm^{-1}symmetric bending of methyl groups, 1383 cm^{-1} relates Ti-O modes [18]. 1368 $cm^{-1}$and 1365 cm^{-1} is due to stretching C-O and C-H bending vibrations, 1224 cm^{-1} and 1261 cm^{-1} asymmetric stretching of the phosphate group, 1171 cm^{-1} showsC-O-O-C asymmetric stretching, 1145 cm^{-1} C-OH bond vibration, 1028 cm^{-1} C-OH deformation [17]. Absorption band between 500 and 1000 cm ascribed to the vibration absorption of the Ti–O–Ti linkages in Titanium dioxide nanoparticles [19].

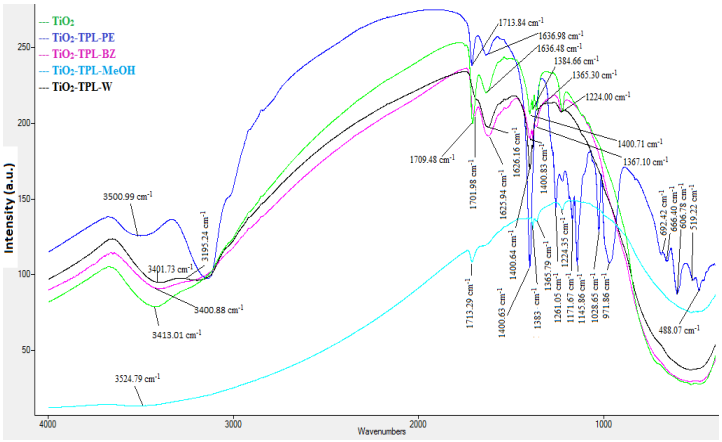

Figure 4. FTIR Spectrum of the samples.

Absorption spectrum obtained by UV. Visible spectra were observed below the region 400 nm wavelength while the smooth decay observed towards the wavelengths above 400 nm, which is influenced by their size, morphology and surface chemistry (Figure 5). The absorption spectrum depicts hypsochromic shift, i.e. absorption in shorter wavelength. A shift towards the blue region attributes to decreased crystallite size [20]. The absorption peaks observed around 270- 290 nm due to the extinction absorption band. As the function of photon energy, absorption band edges extrapolated to calculate indirect bandgap, which found to be around 3.26 eV [21-23].

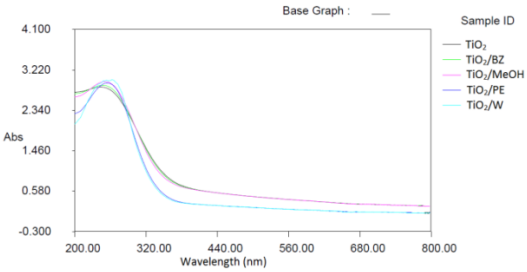

Figure 5. The UV-Visible spectra of synthesized nanoparticles.

According to Courtecuisse et al., (1996), the formation of TiO_2 by the reaction of Titanium alkoxide and alcohol is due to the dehydration of alcohol followed by the hydrolysis of Titanium alkoxide [24]. They proposed the following reaction mechanism, which may reveal the synthesis of TiO2 in the present study:

$$CH_3CH_2OH \rightleftharpoons CH_2{=}CH_2 + H_2O \quad (1)$$

$$Ti\,[OCH\,(CH_3)_2]_4 + H_2O \rightleftharpoons Ti\,[OCH\,(CH_3)_2]_3\,(OH) + (CH_3)_2CHOH \quad (2)$$

$$Ti\,[OCH\,(CH_3)_2]_3 + H_2O \rightleftharpoons Ti\,[OCH\,(CH_3)_2]_2\,(OH)_2 + (CH_3)_2CHOH \quad (3)$$

$$Ti\,[OCH\,(CH_3)_2]_3 + H_2O \rightleftharpoons Ti\,[OCH\,(CH_3)_2]\,(OH)_3 + (CH_3)_2CHOH \quad (4)$$

$$Ti\,[OCH\,(CH_3)_2]\,(OH)_3 \rightarrow TiO_2 + H_2O + (CH_3)_2CHOH \quad (5)$$

Titanium hydroxide formed in reaction 4 is unstable; therefore, it undergoes decomposition to form TiO_2. Reaction (5) shows the formation of TiO_2 via thermal decomposition of titanium hydroxide. Similarly, green synthesis of TiO_2 nanoparticles took

place; here, phytophenolic compounds may serve as capping as well as the reducing agent [25]. Capping and reducing agents has an important role in the formation of nanoparticles. Most of the protocols for chemical synthesis depend upon the use of heteroatom functionalized long-chain hydrocarbons which may exert an adverse effect on the environment. Green synthesis protocol is concerned for the less hazardous and energy-saving capping agents. As far as reducing agents have been concerned, plant-based reducing agents are favourable because of the presence of several polysaccharides, amino acids, proteins and enzymes [26].

3.2. Antimicrobial activity of extracts.

The antimicrobial activity measured in terms of ZOI (zone of inhibition) that includes the 6mm diameter of the well/disk. The crude extract of four different solvents, namely petroleum ether, benzene, methanol and water, were tested. Results revealed that methanolic as well as water extracts were predominantly active against all the test organisms, whereas benzene extract gave the least activity. Water extract shows the maximum zone of inhibition against *Pseudomonas aeruginosa* MTCC 2474 (11.33±0.33 mm) followed by *Escherichia coli* MTCC 40 (10±0 mm) and *Streptococcus pyogenes* MTCC 442 (7±0 mm). The methanol extracted leaves gave maximum activity against *Escherichia coli* MTCC 40 (11±0.57 mm) followed by *Pseudomonas aeruginosa* MTCC 2474 (8.66±0.33 mm) and *Streptococcus pyogenes* MTCC 442 (8.33±0.33 mm). Similarly, Petroleum ether extract gave the maximum zone of inhibition against *Streptococcus pyogenes* MTCC 442 (11.66±0.33) followed by *Escherichia coli* MTCC 40 (10±0.57) and no zone of inhibition was shown against *Pseudomonas aeruginosa* MTCC 2474. Benzene extract gave similar inhibition against *Pseudomonas aeruginosa* MTCC 2474 and *Streptococcus* pyogenes MTCC 442 (9±0.57), and there was no inhibition zone observed against the *Escherichia coli* MTCC 40. Figure (6).

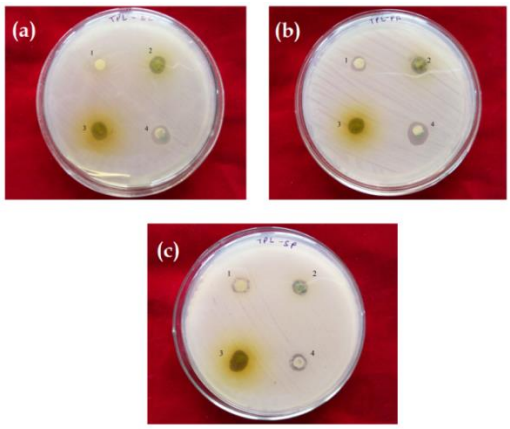

Figure 6. Antibacterial efficacy of crude extracts (1.Benzene, 2. Water, 3. Petroleum ether and 4. Methanol)of *Tephrosiapurpurea* leaves against (a) *Escherichia coli* MTCC 40, (b) *Pseudomonas aeruginosa* MTCC 2474 and (c) *Streptococcus pyogenes* MTCC 442.

3.3. Antimicrobial activity of nanoparticles.

Chemically synthesized nanoparticles gave quite similar results with each other having a zone of inhibition approximately 12 mm against all the test organisms. Figure 7 (a), 7 (b), 7(c) shows the antibacterial screening of chemically synthesized nanoparticles against different test organisms whereas figure 8(a), 8(b) and 8 (c) shows the antibacterial efficacy of crude extracts of Tephrosiapurpurea leaves and antibiotics against different test organisms. Among green synthesized nanoparticles TiO_2/PE nanoparticles showed the best bactericidal activity against each test organism.

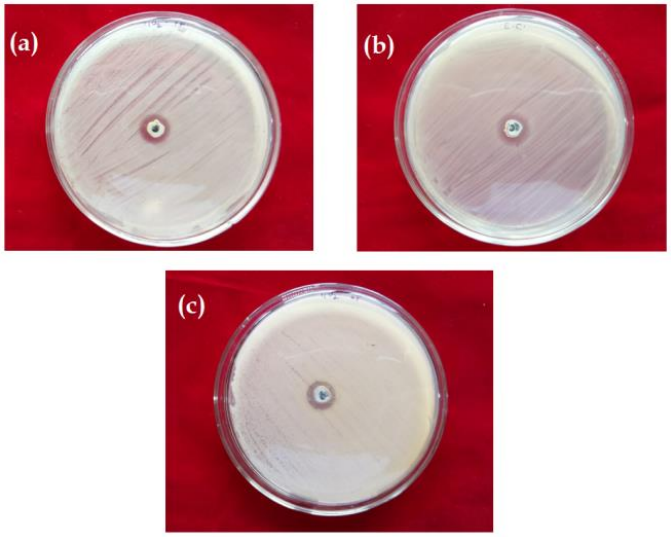

Figure 7. Antibacterial screening of chemically synthesized nanoparticles against (a) *Pseudomonas aeruginosa* MTCC 2474, (b) *Escherichia coli* MTCC 40 and (c) *Streptococcus pyogenes* MTCC 442.

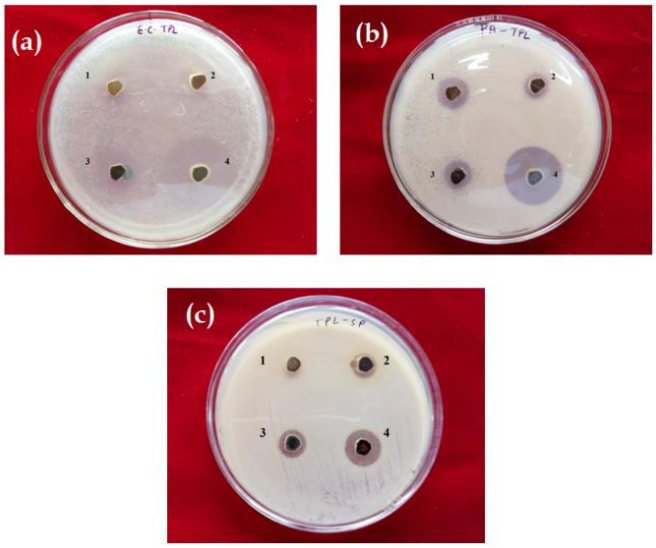

Figure 8. Antibacterial screening of green synthesized nanoparticles(1. TiO_2/Benzene, 2. TiO_2/Water, 3. TiO_2/Petroleum ether and 4. TiO_2/Methanol) against (a) *Escherichia coli MTCC* 40, (b) *Pseudomonas aeruginosa* MTCC 2474 and (c) *Streptococcus pyogenes* MTCC 442.

It gives (27±0.57 mm) inhibition zone for *Escherichia coli* MTCC 40 followed by *Pseudomonas aeruginosa* MTCC 2474 (24±0.57 mm) and *Streptococcus pyogenes* MTCC 442 (15±0.57 mm). Whereas TiO_2/MeOH nanoparticles gave maximum inhibition zone for *Escherichia coli* MTCC 40 (16.33±0.33 mm) followed by *Pseudomonas aeruginosa* MTCC 2474 (13.6±0.33 mm) and *Streptococcus pyogenes* MTCC 442 (11.33±0.33). TiO_2/W nanoparticles gave (12±0 mm) zone of inhibition against *Pseudomonas aeruginosa* MTCC 2474 followed by *Escherichia coli* MTCC 40 (10±0 mm) and there was no inhibition seen against *Streptococcus pyogenes* MTCC 442. Maximum zone of inhibition by TiO_2/BZ nanoparticles observed against *Pseudomonas aeruginosa* MTCC 2474 (15.66±0.33 mm) followed by *Streptococcus pyogenes* MTCC 442 (11.33±0.33) and *Escherichia coli* MTCC 40 (09±0.57). The commonly used antibiotics i.e. Ampicillin, Cefazolin and Streptomycin against wound infection

causing pathogens were used as a positive control. Figure 9 (a), 9 (b) and 9 (c) Show the antibacterial screening of positive control against all the test organisms. Ampicillin gave maximum inhibition zone for *Escherichia coli* MTCC 40 (20±0.57 mm) followed by *Pseudomonas aeruginosa* MTCC 2474 (15±0 mm) and *Streptococcus pyogenes* MTCC 442 (7.66± 0.33). Cefazolin gave maximum inhibition against *Escherichia coli* MTCC 40 (24±0.57 mm) followed by *Pseudomonas aeruginosa* MTCC 2474 (12±0 mm) and *Streptococcus pyogenes* MTCC 442 (7±0 mm) whereas Streptomycin showed maximum activity against Pseudomonas aeruginosa MTCC 2474 (36±0 mm) followed by *Escherichia coli* MTCC 40 (25.66±0.57) and *Streptococcus pyogenes* MTCC 442 (14±0 mm).

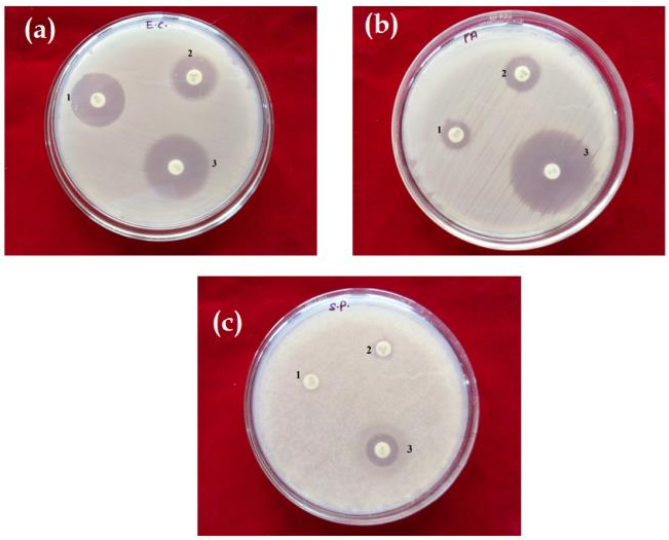

Figure 9. Antibacterial screening of antibiotics (1. Cefazolin (30mcg), 2. Ampicillin (10 mcg) andStreptomycin (10 mcg) against (a) *Escherichia coli* MTCC 40, (b) *Pseudomonas aeruginosa* MTCC 2474 and (c) *Streptococcus pyogenes* MTCC 442.

All the values of the zone of inhibition include the diameter of cork borer and disks used for the antibacterial activity. The antimicrobial activities of different samples with the zone of inhibitions represented by the figure 10.

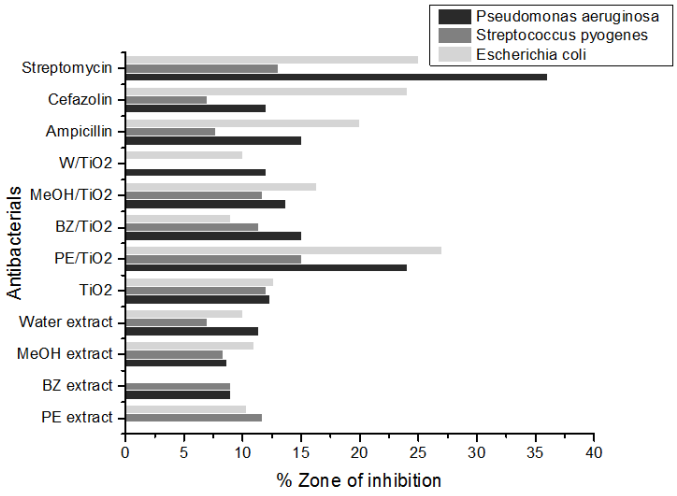

Figure 10. Graphical representation shows the comparison of the zone of inhibition between antimicrobial agents used against *Pseudomonas aeruginosa*, *Streptococcus pyogenes* and *Escherichia coli.*

As the TiO_2/PE nanoparticles gave maximum antimicrobial efficacy against *Escherichia coli* MTCC 40, therefore its antimicrobial results were analyzed by FESEM technique to observe the change in morphology of the bacteria. Figure 11 explained the morphological variations; the untreated *Escherichia coli* cells were in their natural shape while colossal damage in the cell wall observed in the treated cells. On comparison of antibacterial activity of crude extracts with chemically synthesized and green synthesized nanoparticles, we found that green synthesized nanoparticles showed more potential. Especially, TiO_2/PE nanoparticles gave the best activity against all tested pathogens. In comparison with three standard antibiotics, we found that except TiO_2/W all the green synthesized nanoparticles gave better results than cefazoline and ampicillin but not more than streptomycin. The synthesized nanoparticles utilized for their antimicrobial potential were in anatase phase as previously mentioned.

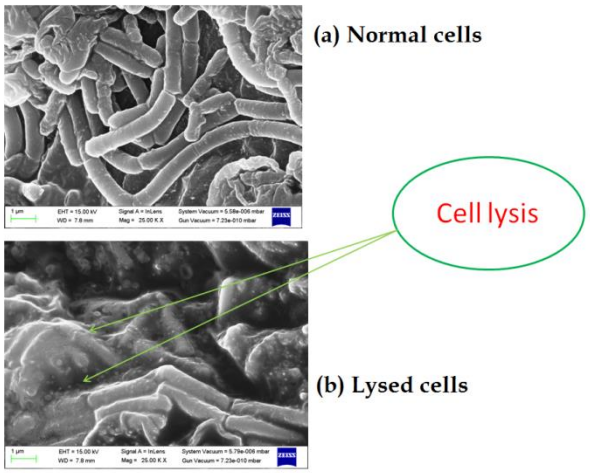

Figure 11. Shows the morphology of the bacteria (A) before treatment and (B) after the treatment by nanoparticles.

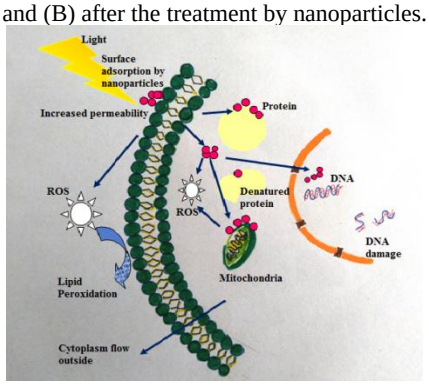

Figure 12. Shows the outline of cell damage due to the ROS effect by TiO_2nanoparticles.

Actually, the anatase phase of titanium dioxide nanoparticles has a bandgap of 3.2 eV, which makes anatase the most active form of titanium dioxide. It produces reactive species due to the result of the photocatalytic reaction and causing microbial cell damage [27]. Direct electron transfer could take place between the cell and the titanium dioxide when the particles are attached to the cell surface. A very small sized particle can penetrate the cell, which results in the transfer of electrons inside the cell. The light would be an essential factor for the photocatalytic activity if it came from any ultraviolet source leading to the direct photochemistry. Photocatalysis can also be enhanced by irradiation of light on microbe while it adsorbed on the oxide surface [28]. Therefore, the synthesized nanoparticles irradiated with ultraviolet radiations before performing the antimicrobial activity. The antibacterial activity may be due to the interaction of ROS (reactive oxygen

species) with lipid membranes which causes peroxidation of lipids leading to the rupture of cell membrane causing the death of the cell (Figure 11). ROS generation maybe because of efficiency in the production of OH in the anatase phase of TiO_2 nanoparticles [29-30]. Upon interacting with the cell anatase phase of TiO2 nanoparticles produces OH radicals which are highly reactive, that's why they are short-lived. At the moment of their generation, they immediately comes in contact with the exterior surface of the bacteria until the titanium dioxide particles penetrate the cell [27]. Figure 12 shows the schematic representation of the cell damage due to ROS.

The following steps can summarize cell damage by the nanoparticles:

- The ROS production by the titanium dioxide nanoparticles induces the electron-hole pair under the radiation.
- Because of electrostatic force generated by the large surface of nanoparticles, they attached to the cell surface of the bacteria, causing peroxidation leading to the cell wall damage.

As the cell wall gets damaged, cytoplasm flows out helping nanoparticles to get entered inside the cell following the damage to the cell organelles [31].

4. CONCLUSIONS

TiO_2 nanoparticles successfully synthesized by using crude extracts of the plant. Green synthesized nanoparticles gave potential antibacterial activity which is comparable with standard drugs available in the market. According to the results, we can conclude that green synthesized nanoparticles have much more antimicrobial potential as compared to chemically synthesized and crude extracts of medicinal plants. This eco-friendly approach is economical as well as cost-effective might be one of the alternatives of conventional medicines against the skin and wound.

5. REFERENCES

1. Lombardo, D; Kiselev, M.A.; Caccamo, M.T. Smart nanoparticles for drug delivery application: development of versatile nanocarrier platforms in biotechnology and nanomedicine. *Journal of Nanomaterials* **2019**, *2019*, 1-26, https://doi.org/10.1155/2019/3702518.
2. Fathi-Achachelouei, M.; Knopf-Marques, H.; Ribeiro da Silva, C.E.; Barthès, J.; Bat, E.; Tezcaner, A.; Vrana, N.E. *Frontiers in bioengineering and biotechnology* **2019,** *7*, 1-22, https://doi.org/10.3389/fbioe.2019.00113.
3. Swaminathan M.; Sharma N.K. Antimicrobial Activity of the Engineered Nanoparticles Used as Coating Agents. In: *Book Handbook of Ecomaterials*. Eds. 1; Springer, Cham, Switzerland, Volume 1. 2019; pp. 549-563, https://doi.org/10.1007/978-3-319-68255-6_1.
4. Pawar, M.; Topcu Sendoğdular, S.; Gouma, P. A Brief Overview of TiO2 Photocatalyst for Organic Dye Remediation: Case Study of Reaction Mechanisms Involved in Ce-TiO2 Photocatalysts System. *Journal of Nanomaterials* **2018,** *2018*, 1-13, https://doi.org/10.1155/2018/5953609.
5. US Food and Drug Administration. 2019. CFR-code of federal regulations title 21. https://www.accessdata.fda.gov/scripts/cdrh/cfdocs/cfcfr/cfrsearch.cfm retrived on 9 February 2020.
6. Ripolles-Avila, C.; Martinez-Garcia, M.; Hascoët, A.-S.; Rodríguez-Jerez, J.J. Bactericidal efficacy of UV activated TiO2 nanoparticles against Gram-positive and Gram-negative bacteria on suspension. *CyTA - Journal of Food* **2019**, *17*, 408-418, https://doi.org/10.1080/19476337.2019.1590461.
7. Lodhi, S.; Pawar, R.S.; Jain, A.P.; Singhai, A.K. Wound healing potential of Tephrosia purpurea (Linn.) Pers. in rats. *Journal of Ethnopharmacology* **2006**, *108*, 204-210, https://doi.org/10.1016/j.jep.2006.05.011.
8. Babu, N.; Singh, A.; Singh, R. A review on therapeutic potential and phytochemistry of *Tephrosia purpurea*. *Bulletin of Pure & Applied Sciences-Botany* **2017**, *36*, 91-104, https://doi.org/10.5958/2320-3196.2017.00013.1.
9. Altemimi, A.; Lakhssassi, N.; Baharlouei, A.; Watson, G.D.; Lightfoot, A.D. Phytochemicals: Extraction, Isolation, and Identification of Bioactive Compounds from Plant Extracts. *Plants* **2017**, *6*, 1-23, https://doi.org/10.3390/plants6040042.
10. Liu, H.; Yang, W.; Ma, Y.; Cao, Y.; Yao, J.; Zhang, J.; Hu, T. Synthesis and Characterization of Titania Prepared by Using a Photoassisted Sol−Gel Method. *Langmuir* **2003**, *19*, 3001-3005, https://doi.org/10.1021/la026600o.
11. Balouiri, M.; Sadiki, M.; Ibnsouda, S.K. Methods for in vitro evaluating antimicrobial activity: A review. *Journal of Pharmaceutical Analysis* **2016**, *6*, 71-79, https://doi.org/10.1016/j.jpha.2015.11.005.
12. Maurya, A.; Chauhan, P.; Mishra, A.; Pandey, A.K. Surface functionalization of TiO2 with plant extracts and their combined antimicrobial activities against *E. faecalis* and *E. coli*. *Journal of Research Updates in Polymer Science* **2012**, *1*, 43-51, http://dx.doi.org/10.6000/1929-5995.2012.01.01.6.
13. Mobeen Amanulla, A.; Sundaram, R. Green synthesis of TiO2 nanoparticles using orange peel extract for antibacterial, cytotoxicity and humidity sensor applications. *Materials Today: Proceedings* **2019**, *8*, 323-331, https://doi.org/10.1016/j.matpr.2019.02.118.
14. W.H. Impact of agglomeration state of nano- and submicron sized gold particles on pulmonary inflammation. *Particle and Fibre Toxicology* **2010**, *7*, 1-37, https://doi.org/10.1186/1743-8977-7-37.
15. Caldorera-Moore, M.; Guimard, N.; Shi, L.; Roy, K. Designer nanoparticles: incorporating size, shape and triggered release into nanoscale drug carriers. *Expert Opinion on Drug Delivery* **2010**, *7*, 479-495, https://doi.org/10.1517/17425240903579971.
16. Thanh, N.T.K.; Maclean, N.; Mahiddine, S. Mechanisms of Nucleation and Growth of Nanoparticles in Solution. *Chemical Reviews* **2014**, *114*, 7610-7630, https://doi.org/10.1021/cr400544s.
17. Movasaghi, Z.; Rehman, S.; ur Rehman, D.I. Fourier Transform Infrared (FTIR) Spectroscopy of Biological Tissues. *Applied Spectroscopy Reviews* **2008**, *43*, 134-179, https://doi.org/10.1080/05704920701829043.
18. León, A.; Reuquen, P.; Garín, C.; Segura, R.; Vargas, P.; Zapata, P.; Orihuela, A.P. FTIR and Raman Characterization of TiO2 Nanoparticles Coated with Polyethylene Glycol as Carrier for 2-Methoxyestradiol. *Applied Sciences* **2017**, *7*, 1-9, https://doi.org/10.3390/app7010049.
19. Lu, X.; Lv, X.; Sun, Z.; Zheng, Y. Nanocomposites of poly(l-lactide) and surface-grafted TiO2 nanoparticles: Synthesis and characterization. *European Polymer Journal* **2008**, *44*, 2476-2481, https://doi.org/10.1016/j.eurpolymj.2008.06.002.
20. Zhao, L.; Yu, J. Controlled synthesis of highly dispersed TiO2 nanoparticles using SBA-15 as hard template. *Journal of Colloid*

and Interface Science **2006**, *304*, 84-91, https://doi.org/10.1016/j.jcis.2006.08.042.
21. Iwabuchi, A.; Choo, C.-k.; Tanaka, K. Titania Nanoparticles Prepared with Pulsed Laser Ablation of Rutile Single Crystals in Water. *The Journal of Physical Chemistry B* **2004**, *108*, 10863-10871, https://doi.org/10.1021/jp049200d.
22. Jafarkhani, P.; Dadras, S.; Torkamany, M.J.; Sabbaghzadeh, J. Synthesis of nanocrystalline titania in pure water by pulsed Nd:YAG Laser. *Applied Surface Science* **2010**, *256*, 3817-3821, https://doi.org/10.1016/j.apsusc.2010.01.032.
23. Mandal, S.; Jain, N.; Pandey, M.K.; Sreejakumari, S.S.; Shukla, P.; Chanda, A.; Som, S.; Das, S.; Singh, J. Ultra-bright emission from Sr doped TiO2 nanoparticles through r-GO conjugation. *Royal Society open science* **2019**, 6, 190100, https://doi.org/10.1098/rsos.190100.
24. Gourinchas Courtecuisse, V.; Chhor, K.; Bocquet, J.-F.; Pommier, C. Kinetics of the Titanium Isopropoxide Decomposition in Supercritical Isopropyl Alcohol. *Industrial & Engineering Chemistry Research* **1996**, *35*, 2539-2545, https://doi.org/10.1021/ie950584r.
25. Njagi, E.C.; Huang, H.; Stafford, L.; Genuino, H.; Galindo, H.M.; Collins, J.B.; Hoag, G.E.; Suib, S.L. Biosynthesis of Iron and Silver Nanoparticles at Room Temperature Using Aqueous Sorghum Bran Extracts. *Langmuir* **2011**, *27*, 264-271, https://doi.org/10.1021/la103190n.
26. Duan, H.; Wang, D.; Li, Y. Green chemistry for nanoparticle synthesis. *Chemical Society Reviews* **2015**, *44*, 5778-5792, https://doi.org/10.1039/C4CS00363B.
27. Wang, P.; Li, K.; Qian, J.; Wang, C.; Lu, B.; Tian, X.; Jin, W.; He, X. Differential toxicity of anatase and rutile TiO2 nanoparticles to the antioxidant enzyme system and metabolic activities of freshwater biofilms based on microelectrodes and fluorescence in situ hybridization. *Environmental Science: Nano* **2019**, *6*, 2626-2640, https://doi.org/10.1039/C9EN00389D.
28. Jin, C.; Su, K.; Tan, L.; Liu, X.; Cui, Z.; Yang, X.; Li, Z.; Liang, Y.; Zhu, S.; Yeung, K.W.K.; Wu, S. Near-infrared light photocatalysis and photothermy of carbon quantum dots and au nanoparticles loaded titania nanotube array. *Materials & Design* **2019**, *177*, https://doi.org/10.1016/j.matdes.2019.107845.
29. Łabuz, P.; Gryboś, J.; Pietrzyk, P.; Sobańska, K.; Macyk, W.; Sojka, Z. Photogeneration of reactive oxygen species over ultrafine TiO2 particles functionalized with rutin–ligand induced sensitization and crystallization effects. *Research on Chemical Intermediates* **2019**, *45*, 5781-5800, https://doi.org/10.1007/s11164-019-04002-z.
30. Zoltan, T.; Rosales, M.C.; Yadarola, C. Reactive oxygen species quantification and their correlation with the photocatalytic activity of TiO2 (anatase and rutile) sensitized with asymmetric porphyrins. *Journal of Environmental Chemical Engineering* **2016**, *4*, 3967-3980, https://doi.org/10.1016/j.jece.2016.09.008.
31. Hou, J.; Wang, L.; Wang, C.; Zhang, S.; Liu, H.; Li, S.; Wang, X. Toxicity and mechanisms of action of titanium dioxide nanoparticles in living organisms. *Journal of Environmental Sciences* **2019**, *75*, 40-53, https://doi.org/10.1016/j.jes.2018.06.010.

6. ACKNOWLEDGEMENTS

RGNF for SC financially supported this research.